An Improvement on Maximum Entropy Analysis of Photon Correlation Spectroscopy Data

Chang-De Sun,† Zhulun Wang, Guangwei Wu, and Benjamin Chu*

Department of Chemistry, State University of New York at Stony Brook, Stony Brook, New York 11794-3400

Received January 2, 1991; Revised Manuscript Received September 23, 1991

ABSTRACT: The maximum entropy method (MEM) has been applied to the analysis of intensity autocorrelation data using photon correlation spectroscopy. However, its effectiveness in terms of resolution, reliability, and applicability is often limited by the details of the mathematical techniques used in the formalism. For example, its success could depend on our understanding of the physical processes governing the data output and the corresponding appropriate constraints specified in the maximum entropy method. Here, we present an improvement on a crucial constraint in the maximum entropy method, i.e., a new form for the error estimation: $\sigma_i^2 = d_i^{0.05}/4B$, with σ_i^2 being the standard square deviation of data d_i and B being a measured base line based on the self-beating technique. An exponent of 0.05 was obtained on the basis of the approximate computing method. The overall improvement has been tested by analyzing both numerically simulated correlation data, including unimodal and various bimodal characteristic line width distributions, and experimental data of binary and ternary polymer solutions. When compared with the CONTIN method by Provencher and another MEM formalism using an application of Bayesian statistics, better fitting of data with lower, more random residuals and better reconstructed characteristic line width distributions were achieved, especially for very closely spaced bimodal distributions.

I. Introduction

In polymer solutions, measurements of the angular distribution of the spectrum of scattered light by means of photon correlation spectroscopy permit us to investigate the dynamics of a variety of polymers in solution.[1] In the self-beating mode, the intensity time correlation function $G^{(2)}(\tau)$ is related to the normalized first-order electric field correlation function $g^{(1)}(\tau)$ by the Siegert relation

$$G^{(2)}(\tau) = B(1 + \beta|g^{(1)}(\tau)|^2) \quad (1)$$

where B is the baseline and β is a coherence factor. For polydisperse structureless particles, $g^{(1)}(\tau)$ has the form

$$|g^{(1)}(\tau)| = \int_0^\infty G(\Gamma)\, e^{-\Gamma\tau}\, d\Gamma \quad (2)$$

where Γ ($=DK^2$) is a characteristic line width, with D and K being a translational diffusion coefficient and the magnitude of a scattering vector, respectively, and $G(\Gamma)$ is the normalized characteristic line width distribution. Equation 2 is a Fredholm integral equation of the first kind.[2] Laplace inversion of eq 2 is used to retrieve the normalized characteristic line width distribution $G(\Gamma)$. However, due to the bandwidth limitation, i.e., there is a minimum delay time τ_{min} and a maximum delay time τ_{max} for a photon correlation instrument, and unavoidable noises as well as a limited number of data points, the measured $g^{(1)}(\tau)$ is always less than that needed to describe $G(\Gamma)$ uniquely. The above Laplace inversion becomes a well-known ill-posed problem.

There are many approaches to solve such an ill-posed problem. For example, in small-angle X-ray scattering (SAXS) an extrapolation method has been used.[3] Some model functions have been chosen to represent $G(\Gamma)$ approximately, such as a log-normal distribution function in evaluating SAXS parameters by transmission electron microscopy.[4] Among the various approaches, the maximum entropy method offers promise for further improvements.

From the information theory, Jaynes[5] and Levine[6] proved that the maximum entropy analysis was very reliable, especially during the analysis of those nonlinear inversion problems in which only an approximate solution instead of an analytical solution could satisfy the constraint conditions in the MEM.

Livesey et al.[7,8] applied the MEM to analyze experimental data from quasi-elastic light scattering and pulse-fluorometry measurements. Nyeo and Chu[9] recently reviewed the MEM and applied it to data analysis of photon correlation spectroscopy (PCS). The MEM has been used successfully in investigating the relationship between the structure factor and the electron density distribution of crystals by means of X-ray diffraction.[10-14] Potton et al.[15] obtained unimodal, bimodal, and trimodal distributions by using the MEM in an analysis of their small-angle neutron scattering data. Moreover, they demonstrated that the MEM could provide a correlation to any resolution of slit smearing in X-ray scattering studies. The MEM has also been applied successfully in reconstructions of two-dimensional nuclear magnetic resonance (NMR) spectra,[16] image in radio space telescopes,[17] and particle-sizing analysis in magnetic granuclometry.[18]

We have applied the MEM in analysis of PCS data of polymer solutions. Normally, the quadratic model approach[9] works well in the Lagrange optimization with a χ^2 constraint. However, it deteriorates with decreasing signal to noise ratio and has limited resolution for multimodal distributions. By careful examination of the mathematical approaches used in the MEM, we found that the form of the standard square deviation σ_i^2 could be improved. Based on physical and mathematical analysis, we obtained a better analytical form for σ_i^2. To evaluate the reliability of the modified MEM, we applied it to simulated data. In comparison with the previous MEM[9] and more recent MEM developments using an application of Bayesian statistics[19-21] as well as the CONTIN approach,[22] our MEM appears to show a higher resolution.

The present paper is organized as follows. In section II, the principle of the maximum entropy formalism is

* To whom all correspondence should be addressed.
† On leave from the Department of Physics, Peking University, Beijing, PRC.

0024-9297/92/2225-1114$03.00/0

reviewed. The modification of σ_i^2 is presented in section III, and the application of the modified MEM to both simulated and experimental data is discussed in section IV. Finally, we conclude in section V.

II. Principle of Maximum Entropy

There are many approximate methods to solve the inverse problem. The maximum entropy formalism, based on the general information theory, is an effective method which produces objective and consistent solutions.[5,6] The essential formalism used in the MEM is the probability theory in statistical mechanics. The result of maximization of system entropy provides reliable information even based on incomplete data.[19-21,23] The details of the MEM formalism and its application to analyze PCS data have been discussed elsewhere.[9] In brief, we review the application of the MEM to analyzing PCS data.

According to eq 1, the measured net intensity correlation function data d_i^2 in PCS could be expressed as

$$d_i^2 = \beta|g^{(1)}(\tau_i)|^2 \tag{3}$$

To get an estimate $\hat{G}(\Gamma)$ of the true characteristic line width distribution $G(\Gamma)$ from the obtained experimental data, we first consider the discrete case

$$\hat{d}_i = \sum_{j=1}^{N} F_j K_{ij} \tag{4}$$

where $K_{ij} = \exp(-\Gamma_j \tau_i)$ is the curvature matrix, $F_j = \hat{G}(\Gamma_j)\Gamma_j\Delta$ is a distribution function in log Γ spacing, $\Delta = (\ln \Gamma_N - \ln \Gamma_1)/(N-1)$ is the constant increment in log Γ spacing, and N is the number of function values $\hat{G}(\Gamma_j)$ used in the discretization approximation. Livesey[7] proved that the prior distribution should be considered as a constant b in the maximum entropy formalism under the above condition. Thus, we have an entropy S of the system

$$S = -\sum_{j=1}^{N}\{F_j \ln (F_j/b)\} = -\sum_{j=1}^{N}\{F_j \ln (F_j/A_0) - F_j\} \tag{5}$$

where the constant A_0 ($=b/e$ with $e = 2.718...$) is a default or predetermined value. We choose $A_0 = \sqrt{\beta}/N$; thus, F_j and A_0 are normalized to $\sqrt{\beta}$, which is the case for PCS characteristic line width distributions. The measured datum d_i is related to the estimated datum $\hat{d}_i$ by a certain statistical criterion, i.e., the χ^2 constraint which we consider as

$$\chi^2 = \sum_{i=1}^{M}\left(\frac{\hat{d}_i - d_i}{\sigma_i}\right)^2 = M \tag{6}$$

where σ_i^2 represents the error square deviation and M is the number of data points. In general, we can obtain the maximum entropy (eq 5) of the system subject to the χ^2 constraint (eq 6) based on eqs 4–6. This is a variational optimization problem with χ^2 as the constraint, and the problem could be solved by several standard approaches.

In the method of Lagrange multipliers, the established Lagrangian is

$$L(F_j) = S - \frac{\alpha}{2}\chi^2 \tag{7}$$

with α (>0) being an undetermined Lagrange multiplier. In order to improve the precision of the computation, we expand S and χ^2 to the second term based on the quadratic model approximation approach:

$$\hat{S} = S_0 + \sum_{j=1}^{N}(\partial S/\partial F_j)\,\delta F_j + {}^1/_2 \sum_{j,K}^{N}(\partial^2 S/\partial F_j\,\partial F_K)\,\delta F_j\,\delta F_K \tag{8}$$

$$\hat{\chi}^2 = \chi_0{}^2 + \sum_{j=1}^{N}(\partial\chi^2/\partial F_j)\,\delta F_j + {}^1/_2 \sum_{j,K}^{N}(\partial^2\chi^2/\partial F_j\,\partial F_K)\,\delta F_j\,\delta F_K \tag{9}$$

The quadratic model is expanded about $F_j^0 = A_0$. To make the expansion convergent, we require the third term to be smaller than the first and second terms. It is necessary to set an upper bound on the quadratic term

$$\sum_{j,K}^{N}(\partial^2 S/\partial F_j\,\partial F_K)\,\partial F_j\,\partial F_K \le 0.1\sum_{j}^{N} F_j^0 \tag{10}$$

where 0.1 is an empirical constant chosen based on practical experience. Equation 10 is one of the criteria in the computation.

To make the computation convenient, the variable F_j is usually converted to an orthogonal vector and a corresponding Lagrangian can be established in the new orthogonal coordinate. Similarly, the χ^2 constraint has its expression in the orthogonal coordinate. Then, the solution to MEM can be obtained. During the computation, the solution is searched normally by iteration. In order to approach the χ^2 constraint as defined by eq 6 properly, a slightly higher χ^2 value, which is called $\chi_t{}^2_{arg}$, is imposed in order to provide certain flexibility in the iteration procedure.[9] The $\chi_t{}^2_{arg}$ changes with variation of variables. The value of χ^2 shall be very close to the value of $\chi_t{}^2_{arg}$ in the iteration, which is another criterion in the computation.

Levenberg[24] proposed a condition of $\nabla L = 0$ in the analysis of nonlinear maximization problems. Physically, the zero of the gradient of a scalar indicates that the scalar has a stable tendency. Therefore, the solution shall also be stable. Burch et al.[25] and Skilling et al.[26] reported a similar approach and explanation. Furthermore, it is suggested in ref 9 that

$$\sum_{j=1}^{N} F_j[\alpha_1(\partial S/\partial F_j) - \alpha_2(\partial\chi^2/\partial F_j)]^2 < 2\times 10^{-2} \tag{11}$$

which guarantees the stability of the solution. The entire Lagrangian scalar could be in a stable state if the difference between the gradient of entropy and the gradient of χ^2 is small enough. Here, the choice of a tolerance value of 2×10^{-2} is based on the number of the iterations and on practical grounds. Equation 11 provides the third criterion in the computation of the MEM.

The MEM provides us with a theoretic information approach to the nonlinear inverse problem. The formalism has been successfully applied to various areas. However, if we improve some values of certain variables, e.g., σ_i^2, as a closer reflection to the reality of the problem both mathematically and physically, the MEM can be improved further.

III. Improvement on the σ_i^2 Expression

Livesey[7] formulated the autocorrelation of the scattered light as follows

$$y_i = \text{sign}\,[C_i - B]|C_i - B|^{1/2} \tag{12}$$

where y_i is the electric field correlation function, corre-

sponding to $g^{(1)}(\tau)$ mentioned before where β is assumed to be equal to 1 and C_i corresponding to $G^{(2)}(\tau)$ is the intensity correlation function (ICF). Here, the standard deviation σ_i was considered as Δy_i, i.e., the *estimated* net ICF, $\hat{d}_i^2$, is very close to the *measured* net ICF, d_i^2, at each point. By taking a differential of y_i, i.e., $\Delta y_i = \Delta C_i/2(C_i - B)^{1/2}$, the standard square deviation of the error estimate is given by

$$\sigma_i^2 = \frac{C_i}{4|C_i - B|} \tag{13}$$

in which $(\Delta C_i)^2 = C_i$ by assuming the counting statistics to be Poisson and the original number counts at each point as an estimate of its variance.[7] For the above consideration, σ_i has a differential property. The analytical form of σ^2 used in ref 9 is

$$\sigma_i^2 = \frac{1 + d_i^2}{4Bd_i^2} \tag{14}$$

Equation 14 is an explicit expression of eq 13.

However, based on the fact that in the limit of low count rates the photoelectron counts of light scattering signals obey the Poisson distribution,[27] statistical fluctuations should be introduced to describe the error deviations. There are four assumptions about the events being counted:[28,29] (a) they have no effective upper limit; (b) they occur independent of each other; (c) they occur irregularly; (d) the mean probability of occurrence is a constant. One of the necessary conditions of the Poisson distribution is that the probability of success of events is very small. Also, the mean number of the events is a constant and is equal to the standard deviation σ_i^2. It is not a simple mathematical differential like eqs 13 and 14. The Poisson distribution can be expressed as

$$P_p(x,\mu) = \frac{\mu^x}{x!} e^{-\mu} \tag{15}$$

where P_p is a probability of the Poisson distribution, μ is the mean number of observed events x in unit time, and x is the number of the observed events every time. In the case of PCS, x corresponds to the characteristic line width Γ_j and μ corresponds to the average characteristic line width $\bar{\Gamma}$. The standard square deviations are

$$\sigma^2 = \overline{(x-\mu)^2} = \sum_{x=0}^{\infty} \left[(x-\mu)^2 \frac{\mu^x}{x!} e^{-\mu} \right] = \mu \tag{16}$$

and the average number of events x is

$$\bar{x} = \sum_{j=1}^{\infty} (x_j P_p(x_j,\mu)) = \mu \tag{17}$$

Thus, μ is a constant here and will not change with the different measured values of x each time. Expression of error deviations by means of a statistical distribution is used not only in light scattering but also in neutron scattering. For example, the statistical error can be calculated by considering the signals to obey a Gaussian distribution[15] for neutron scattering. Therefore, not only does σ_i have a differential property resulting in eq 14 having $\sigma_i^2 \propto d^x$ but it is also a constant according to its Poisson (or Gaussian) distribution. By combining these two features, a new form was given, σ_i^2. The choice of $x = 0.05$ is described in Appendix I.

$$\sigma_i^2 = \frac{1}{4B} d_i^{0.05} \tag{18}$$

The order of the magnitude of net ICF data of polymers in solution is usually in the range of 10^{-1}–10^{-5}, and in this range the fluctuation in the magnitude of $d_{i_2}^{0.05}$ is always on the order of 10^{-1} (see Table I). Then, the constant requirement of σ_i^2 is basically satisfied. However, it is not a pure constant like μ (see Table I). Here, the use of $d_i^{0.05}$ is based upon some experience in approximate computations and upon the above two physical properties of error deviations. Equation 18 represents one of the better choices of the forms of σ_i^2, but it is not the only one.

Table I
Magnitudes of d_i^x

	d_i					
	1×10^{-1}	1×10^{-2}	1×10^{-3}	1×10^{-4}	1×10^{-5}	1×10^{-6}
$x = 0.005$	0.99	0.98	0.97	0.95	0.94	0.93
$x = 0.05$	0.89	0.78	0.71	0.63	0.56	0.50
$x = 0.1$	0.79	0.63	0.50	0.40	0.32	0.25
$x = 0.5$	0.32	0.10	0.032	0.010	0.0032	0.0010

Based on the improved form of σ_i^2, the modified MEM is used to analyze first the simulated correlation data and then the experimental data. By comparing with Provencher's CONTIN algorithm (1984 Version)[22] and MEM (provided by J. Langowski, denoted as MEM-L),[19] we found that our MEM could yield better fitting results in some of the tests we have made.

IV. Applications of Improved MEM

1. Simulation. With simulated data, the base line B was set at 10^7, the instrumental coherence factor $\beta = 0.3$, the maximum characteristic line width $\Gamma_{max} = 1/\tau_1$, and the minimum line width $\Gamma_{min} = 0.01/\tau_M$. The channel number or the number of data points M was taken to be 136. The number of Γ in the distribution was taken to be 81.

The generation of simulated correlation data by computer has been described in ref 9. Briefly, the following log-normal function was used in the generation

$$G(\Gamma) = G_0(\Gamma) - D \tag{19}$$

$$G_0(\Gamma) = \frac{C}{\Gamma} \exp\left\{ -\frac{1}{\beta^2} (\ln(\Gamma/\Gamma_0))^2 \right\} \tag{20}$$

where C and D are constants, $\beta = [2 \ln(\sigma + 1)]^{1/2}$, $\Gamma_0 = \bar{\Gamma}(\sigma + 1)^{-1/2}$, and $\sigma = \mu_2/\bar{\Gamma}^2$ with $\bar{\Gamma}$ and μ_2 being an approximate mean and the second moment, respectively.

$$\bar{\Gamma} = \int_{\Gamma_{min}}^{\Gamma_{max}} \Gamma\, G(\Gamma)\, d\Gamma \tag{21}$$

$$\mu_2 = \int_{\Gamma_{min}}^{\Gamma_{max}} (\Gamma - \bar{\Gamma})^2\, G(\Gamma)\, d\Gamma \tag{22}$$

Here, the characteristic line width distribution $G(\Gamma)$ is normalized.

$$\int_{\Gamma_{min}}^{\Gamma_{max}} G(\Gamma)\, d\Gamma = 1 \tag{23}$$

The first-order autocorrelation function $g^{(1)}(\tau_i)$ is generated based on eq 2

$$|g^{(1)}(\tau_i)| \approx \sum_{j=1}^{N} \omega_j\, G(\Gamma_j) \exp(-\Gamma_j \tau_i) \Delta \tag{24}$$

where ω_j is a set of constants and $\Delta = (\Gamma_{max} - \Gamma_{min})/(N - 1)$ with N being the total number of equally spaced Γ_j values. Here, we took $N = 1001$ and $\{\omega_j\} = \{1/3, 4/3, 2/3, 4/3, \ldots, 2/3, 4/3, 1/3\}$. Then, the simulated intensity could be derived by eq 3, which is noise-free. To add some random

Table II
Characteristics of Simulated Distribution Functions

ID	$\bar{\Gamma}_1$ (s^{-1})	$\bar{\Gamma}_2$ (s^{-1})	Var_1	Var_2	A_2/A_1	noise	$\bar{\Gamma}$ (s^{-1})/var
S-1	100 (uni)		0.02		0	~0.001	
S-2	100	150	0.001	0.001	0.5	~0.001	121/0.043
S-3	100	200	0.1	0.01	0.5	none	126/0.17
S-4	100	250	0.001	0.001	0.3	~0.01	164/0.21
S-5	100	400	0.001	0.001	0.3	~0.001	264/0.32

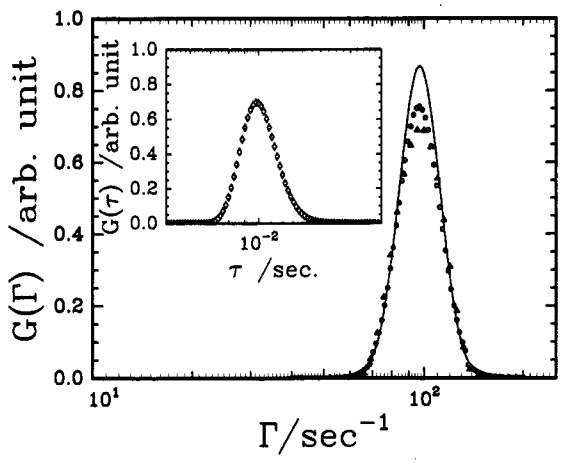

Figure 1. Reconstruction of a unimodal distribution from simulated data with $\bar{\Gamma}$ = 100 s^{-1}, variance 0.02, and added noise of ~0.001. The solid curve, circles, and triangles denote the line width distribution $G(\Gamma)$ from simulation, present MEM output, and CONTIN output, respectively. The inset is a decay time distribution $G(\tau)$ from output of MEM-L.

noise to the generated second-order correlation data, we used the subprograms in the CONTIN algorithm. The noisy correlation data are thus simulated as

$$d_i^2 \text{ (with noise)} = d_i^2 + \text{error } (1 + d_i^2)^{1/2} \qquad (25)$$

where error (=RN/$\sqrt{B}$) is a normal deviate with zero mean and deviation $1/\sqrt{B}$ and RN is a random number.

The above formula and procedures were used in the generation of unimodal distributions. To obtain a simulated bimodal distribution, we simply combined two unimodal cases together. The characteristics of the simulated distribution functions are listed in Table II. In the MEM operation, a linear approximation was introduced to calculate very closely bimodal distributions (see Appendix II). The fitting error could be obtained to within ±0.3%.

1.1. Unimodal Distribution. The method was applied to the simulated correlation data with unimodal distribution first. Figure 1 shows a comparison of input simulated line width distribution with outputs from our MEM, CONTIN, and MEM-L. Basically, all three approaches are equally applicable for unimodal distributions. Table III lists the results of analysis from the above three methods.

1.2. Bimodal Distribution. 1.2.a. Minimum Distance of Two Resolvable Unimodal (δ) Distribution Functions. Figure 2 shows a reconstruction of a bimodal distribution, in which $G(\Gamma)$ contains two unimodal (δ) distribution functions with a ratio $\bar{\Gamma}_2/\bar{\Gamma}_1$ = 1.5 where $\bar{\Gamma}_1$ = 100 s^{-1} and $\bar{\Gamma}_2$ = 150 sec^{-1}; amplitude ratio A_2/A_1 = 0.5; and variances $\mu_{21}/\bar{\Gamma}_1^2$ = 0.001 and $\mu_{22}/\bar{\Gamma}_2^2$ = 0.001. The simulated net ICF data d_i^2 which were derived from eqs 1–3 and added noises by eq 25 were the input to our MEM program as well as to the CONTIN and MEM-L programs for comparison purposes. The computed outputs of reconstructed characteristic line width distributions from our MEM, MEM-L, and the CONTIN method together with the simulated input are displayed in Table III. We

Table III

a. Comparison of Peak Values (s^{-1}) from CONTIN, MEM, and MEM-L Methods

input[a]	CONTIN	MEM	MEM-L[b]
unimodal			
S-1	95.5	96.9	102
exptl data	1.47×10^3	1.45×10^3	1.60×10^3
bimodal			
S-2	120	97.6, 156	127
S-3	100	85.4, 199	81.2, 193
S-4	117	91.4, 214	196
S-5	95.0, 384	96.9, 386	100, 400
exptl data	315, 1.46×10^3	325, 1.40×10^3	393, 1.59×10^3

b. Comparison of $\bar{\Gamma}$ Values (s^{-1}) and Variances from CONTIN and MEM[c]

input[a]	CONTIN	MEM
unimodal		
S-1	100/0.044	100/0.008
exptl data	1.63×10^3/0.084	1.59×10^3/0.053
bimodal		
S-2	122/0.044	102/2.9×10^{-4}, 150/3.1×10^{-4}
S-3	126/0.17	86/9.6×10^{-3}, 204/0.012
S-4	165/0.21	105/0.031, 254/0.031
S-5	102/0.044, 297/0.012	101/0.033, 403/0.019
exptl data	432/0.17, 1.53×10^3/0.029	386/0.12, 1.46×10^3/0.018

[a] Identification number (ID) is used to identify the characteristics of simulated distribution as listed in Table I. [b] Only peak value of the $G(\tau)$ distribution could be obtained from MEM-L. As we received only the executive file of MEM-L in τ space, it is not trivial to convert the results to Γ space. [c] $\bar{\Gamma}$ value (s^{-1})/variance.

found that our MEM was capable of exhibiting a bimodal distribution constructed by two δ functions with A_2/A_1 = 0.5 and $\bar{\Gamma}_2/\bar{\Gamma}_1$ = 1.5, while CONTIN and MEM-L could not. Livesey et al.[7] reported that the best resolution they could obtain from the MEM was the case of A_2/A_1 = 0.5 and $\bar{\Gamma}_2/\bar{\Gamma}_1$ = 2.4. Therefore, our MEM demonstrated higher resolution for analysis of a *closely spaced bimodal* distribution. Under our specified conditions, it goes without saying that the estimated net ICF data $\hat{d}_i^2$ from the MEM fitted the simulated data very well and the fitting residuals (=$(d_i - \hat{d}_i)/\sqrt{\sigma_i^2}$) were randomly distributed.

1.2.b. Minimum Amplitude Ratio of Two Resolvable Unimodal (δ) Functions in the Presence of an Appreciable Amount of Noise. Figure 3 shows a reconstructed bimodal distribution with a small amplitude ratio of A_2/A_1 = 0.3 and a large added noise of 0.01. In general, the characteristic line widths with smaller amplitude ratios are more difficult to be resolved because of more sensitive perturbations from noises in the background or from the noise in the data itself. In addition, the resolving power in the Laplace inversion decreases with increasing noise in the data. In this case, our MEM was still able to retrieve a bimodal distribution although they were not well separated, but CONTIN and MEM-L could provide only a broad distribution. However, it should be noted that all three methods could fit the correlation data well and the fitting residuals were reasonable.

1.2.c. Bimodal Distribution with Two Overlap Peaks. When the two peaks in the bimodal distribution have a certain degree of overlap, the two line widths cannot be resolved easily. By applying our MEM to a simulated bimodal distribution with two overlap peaks of $\bar{\Gamma}_2/\bar{\Gamma}_1$ = 2/1, the reconstructed distribution was able to demonstrate a bimodal feature (see Figure 4). However, the normal MEM failed to resolve such a bimodal distribution even with a larger ratio of two line widths, e.g., $\bar{\Gamma}_2/\bar{\Gamma}_1$ = 3.03 in

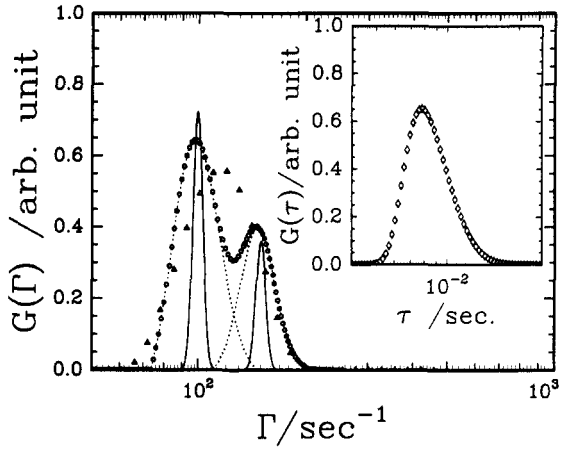

Figure 2. Reconstruction of a bimodal distribution with $\bar{\Gamma}_1$ = 100 s^{-1}, $\bar{\Gamma}_2$ = 150 s^{-1}, and amplitude ratio A_2/A_1 = 0.5. Input variances are 0.001 for both peaks. Solid curves denote the simulated $G(\Gamma)$ distribution. Input signals contained an added noise of ~0.001. Circles represent the output $G(\Gamma)$ distribution from the present MEM, with the dotted curves denoting each of the two separated unimodal (δ) distributions while the triangles represent the CONTIN output. The inset is a decay time distribution $G(\tau)$ from output of MEM-L.

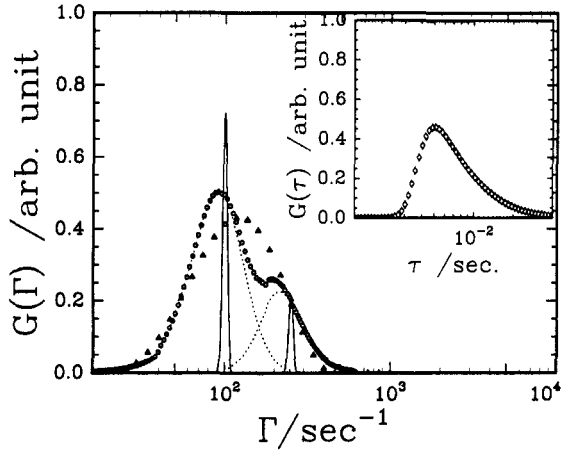

Figure 3. Reconstruction of a bimodal distribution with $\bar{\Gamma}_1$ = 100 s^{-1}, $\bar{\Gamma}_2$ = 250 s^{-1}, and amplitude ratio A_2/A_1 = 0.3. Input variances are 0.001 for both peaks. Solid curves denote the simulated $G(\Gamma)$ distribution. Input signals contained an added noise of ~0.01. Circles represent the output $G(\Gamma)$ distribution from the present MEM, with the dotted curves denoting each of the two separated (δ) distributions while the triangles represent the CONTIN output. The inset is a decay time distribution $G(\tau)$ from output of MEM-L.

ref 9 with the other parameters such as variances and area ratio the same as those in the present condition. The CONTIN method failed in either of the above two cases, while MEM-L could also retrieve the bimodal characteristics in this case. Detailed results are listed in Tables III.

1.2.d. Bimodal Distributions with Two Well-Separated Unimodal (δ) Functions. Finally, we tested the programs for two well-separated unimodal (δ) distributions. All three programs demonstrated almost identical results as shown in Figure 5 with numerical results listed in Tables III.

In summary, tests of our MEM by the simulated data demonstrate that our MEM is reliable and has a greater potential to resolve various types of closely spaced bimodal distributions. In the following section, MEM is used to analyze some experimental PCS data.

2. Experimental Data Analysis. Our MEM was applied to experimentally measured photon correlation

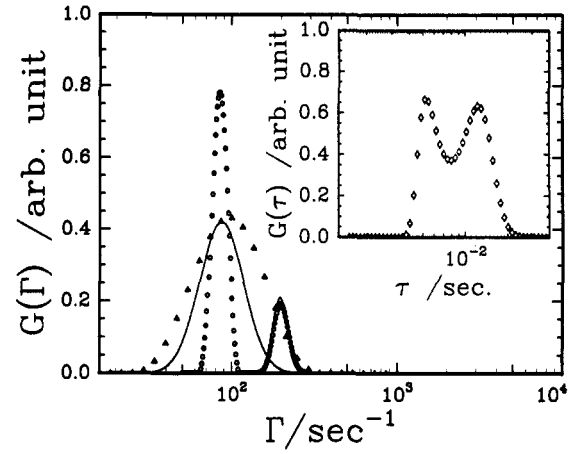

Figure 4. Reconstruction of a bimodal distribution with $\bar{\Gamma}_1$ = 100 s^{-1}, $\bar{\Gamma}_2$ = 200 s^{-1}, and amplitude ratio A_2/A_1 = 0.5. Input variances are 0.1 and 0.01, respectively. Solid curves denote the simulated $G(\Gamma)$ distribution. Circles and triangles represent the output $G(\Gamma)$ distribution from the present MEM and CONTIN, respectively. The inset is a decay time distribution $G(\tau)$ from output of MEM-L.

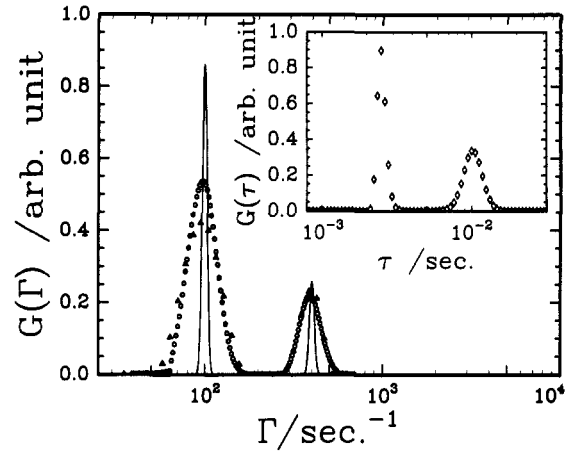

Figure 5. Reconstruction of a bimodal distribution with $\bar{\Gamma}_1$ = 100 s^{-1}, $\bar{\Gamma}_2$ = 400 s^{-1}, and amplitude ratio A_2/A_1 = 0.3. Input variance is 0.001 for both peaks. Solid curves denote the simulated $G(\Gamma)$ distribution. Input signals contained an added noise of ~0.001. Circles and triangles represent the output $G(\Gamma)$ distribution from the present MEM and CONTIN, respectively. The inset is a decay time distribution $G(\tau)$ from output of MEM-L.

Table IV
Characteristics of PS/TOL and PS/PMMA/TOL Polymer Solutions

	$\bar{M}_w$	M_w/M_n	C^* (g/mL)	C_{PS} (g/mL)	C_{PMMA} (g/mL)
PS	3.0×10^5	~1.1	5.3×10^{-2}		
PMMA	9.9×10^6	~1.35	2.5×10^{-3}		
PS/TOL				2.3×10^{-3}	0
PS/PMMA/TOL				2.6×10^{-3}	1.0×10^{-2}

data of a binary solution of monodisperse four-arm star polystyrene (PS) in toluene (TOL) and a ternary solution of a four-arm polystyrene in an entangled linear poly(methyl methacrylate) (PMMA) in toluene. The sample characteristics are listed in Table IV. The photon correlation functions were measured by using a Brookhaven Instruments BI-2030AT digital correlator with 136 channels. The experimental details were described in ref 30.

2.1. Unimodal Distribution. A dilute solution of a monodisperse polymer in a good solvent is expected to display a single characteristic line width with a small

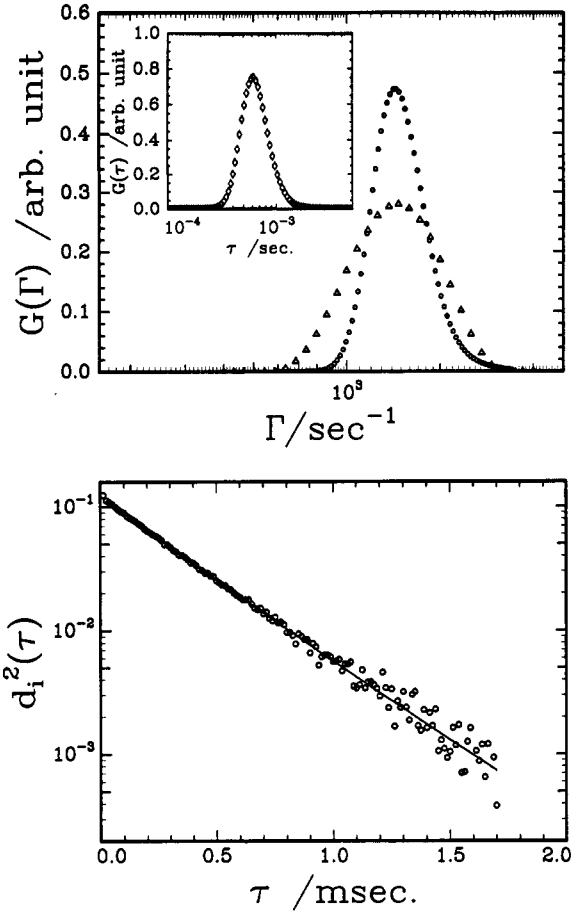

Figure 6. (a, top) Construction of the $G(\Gamma)$ distribution for the binary solution of polystyrene in toluene by MEM, CONTIN, and MEM-L. Circles and triangles denote the output from MEM and CONTIN, respectively. The inset represents the output of MEM-L. (b, bottom) Fittings of time correlation data by using MEM. Circles denote the experimental data, and the line is the output of MEM.

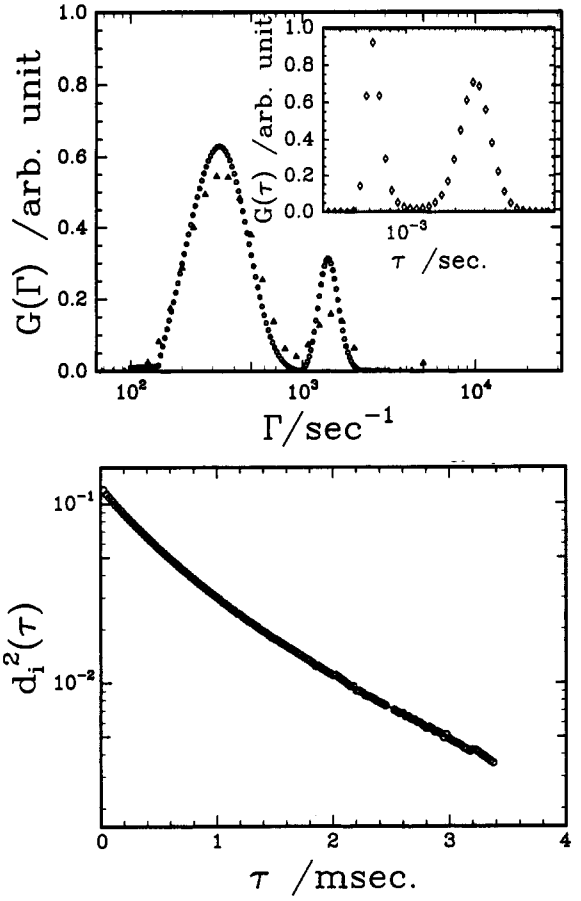

Figure 7. (a, top) Construction of the $G(\Gamma)$ distribution for the ternary solution of polystyrene/PMMA/toluene by MEM, CONTIN, and MEM-L. Circles and triangles denote the output from MEM and CONTIN, respectively. The inset represents the output of MEM-L. (b, bottom) Fittings of time correlation data by using MEM. Circles denote the experimental data, and the line is the output of MEM.

variance at small values of qR where internal motions are not observed. Analysis of the measured PCS data from a dilute solution of polystyrene in toluene by our MEM provided a good fitting to the correlation data and was in good agreement with CONTIN and MEM-L analysis. The results, i.e, reconstructed line width distribution $G(\Gamma)$, intensity data, and its fitting, are shown in Figure 6a,b.

2.2. Bimodal Distribution. In a ternary solution of PS/PMMA/toluene, polymer PMMA was isorefractive with solvent toluene and should be invisible. However, the coupling interaction between polystyrene and PMMA had certain effects on the dynamics of polystyrene and PMMA. Our MEM yielded a bimodal line width distribution for this ternary system which agreed with the CONTIN and the MEM-L result (see Figure 7a). The intensity data were also well fitted as shown in Figure 7b. Applications of our MEM, MEM-L, and CONTIN to the experimental PCS data showed similar results for both unimodal and bimodal distributions. However, under the extreme conditions, our MEM showed a higher resolution than CONTIN and MEM-L could. By using the IBM PS/2 Model 80 computer, the operation time was about ~2 min for each run for our MEM. The overall run time to obtain an appropriate answer to the data analysis depends upon the nature of the input data and can be regarded as comparable (in terms of minutes) for the three methods.

V. Conclusions

In conclusion, the present MEM has several advantages as follows:

1. It could provide good results to various simulated correlation data with unimodal or bimodal characteristic line width distributions.

2. It has a higher resolution for a variety of bimodal distributions than CONTIN, the previous MEM developed by us, and MEM-L. For example, our MEM is able to resolve a bimodal distribution with a ratio of two line widths with $\bar{\Gamma}_2/\bar{\Gamma}_1 \sim 1.5$, while CONTIN could only resolve bimodal distributions with a minimum Γ ratio of ~2.5; the MEM reported by Livesey,[7] a ratio of ~2.4; and MEM-L, a ratio of ~2.0. In the case of a two-overlapped bimodal distribution, our previous MEM[9] could not provide a satisfactory analysis, while the present MEM could.

We have found a key condition (eq 18) which could be used to improve the operations of MEM. It does not mean that MEM cannot be improved further nor does it mean that CONTIN cannot be improved further. Our work suggests that we must understand the physics of the processes we are dealing with and that MEM permits introduction of such appropriate constraints. With better understanding of the processes, more information can be retrieved. This procedure is in agreement with the ill-conditioned nature of the Laplace inversion.

Acknowledgment. B.C. acknowledges support of the research by the U.S. Department of Energy (Grant

DEFG0286 ER45237A005) and the Polymers Program of the National Science Foundation (Grant DMR8921968). B.C. also thanks Dr. J. Langowski, EMBL Grenoble Outstation, France, for sending us his executive file of MEM-L. C.-D.S. thanks Dr. J. Wang for providing assistance in operating the computer.

Appendix I

According to eqs 13 and 14, a more general expression for σ_i^2 can be represented by

$$\sigma_i^2 \propto d_i^x \tag{A-1}$$

where x is an unknown exponent. The expansion of d_i^x is

$$d_i^x = 1 + [(\ln d_i)/1!)]x + [(\ln d_i)^2/2!]x^2 + \ldots + [(\ln d_i)^n/n!]x^n \tag{A-2}$$

The order of magnitude of experimentally measured net ICF data d_i^2 is in the range 10^{-1}–10^{-5}. Thus, we have to find an exponent x to make d_i^x almost constant over such large data range.

In order to choose a value for x, the following requirements need to be satisfied: (a) In the Taylor series expansion, convergence requires $x < 1$. (b) As α should remain close to constant, the value of d^x should be in the same order for the whole range of d varying from 0.1 to ~0.00001 which is an arbitrary choice. For example, x = 0.5 in Table I will not meet this condition. For x = 0.05, the fluctuation in $d_i^{0.05}$ is about constant and has a value of ~0.1, which satisfies condition b. (c) There is an upper bound on the quadratic term (see eq 10). Therefore, we set a similar constraint in the d^x expansion in eq A-2. For example, if x = 0.005, x^2/x = 0.005, which is much smaller than 0.1, while if x = 0.05, x^2/x = 0.05, which is close to 0.1.

Therefore, the choice of x = 0.05 is not unique. We could have used 0.06. It should be noted that if x = 0.1, then condition b will not be as well satisfied as if x = 0.05.

Appendix II

In the extreme case of very closely spaced bimodal distributions, the initial MEM run may yield a bimodal distribution with imperfect shape. The complete bimodal distribution could be obtained by adjusting the running parameters as Γ_{min} and Γ_{max} since the initial choice of $\Gamma_{min} = 0.01/\tau_M$ and $\Gamma_{max} = 1/\tau_1$ may not satisfy the criteria of MEM. However, the adjustment may require many trials. The problem can be solved by introducing a linear approximation; i.e., the bimodal distribution is simply the linear addition of two nonoverlap unimodal distributions. From the initial MEM output distribution, we divided the whole distribution into two parts at the minimum point in the distribution (Γ_{mid}). The corresponding two sets of intensity data $d_i^2{}_1$ and $d_i^2{}_2$ were then input into MEM to obtain the unimodal distributions with the input Γ ranges of Γ_{min}, Γ_{mid} and Γ_{mid}, Γ_{max}, respectively. The final output distribution was the addition of the two unimodal distributions. It was found that the fitted intensity data which was also the linear addition of the two output data sets could agree to within ±0.3% of the input data.

References and Notes

(1) Chu, B. *J. Polym. Sci.: Polym. Symp.* **1985**, *73*, 137–155.
(2) Koppel, D. E. *J. Chem. Phys.* **1972**, *57*, 4814–4820.
(3) Brill, O. L.; Schmidt, P. W. *J. Appl. Phys.* **1968**, *39*, 2274–2281.
(4) Harkness, S. D.; Gould, R. W.; Hren, J. J. *Philos. Mag.* **1969**, *19*, 115–128.
(5) Jaynes, E. T. *Phys. Rev.* **1957**, *106*, 620–630; **1957**, *108*, 171–190.
(6) Levine, R. D. *J. Phys.* **1980**, *A13*, 91–108.
(7) Livesey, A. K.; Licinio, P.; Delaye, M. *J. Chem. Phys.* **1986**, *84*, 5102–5107.
(8) Livesey, A. K.; Delaye, M.; Licinio, P.; Brochon, J. C. *Faraday Discuss. Chem. Soc.* **1987**, *83*, Paper 14.
(9) Nyeo, S.-L.; Chu, B. *Macromolecules* **1989**, *22*, 3998–4009.
(10) Sakata, M.; Sato, M. *Acta Crystallogr.* **1990**, *A46*, 263–270.
(11) Bricogne, G.; Gilmore, C. J. *Acta Crystallogr.* **1990**, *A46*, 284–297.
(12) Prince, E. *Acta Crystallogr.* **1989**, *A45*, 200–203.
(13) Prince, E.; Sjolin, L.; Alenljung, R. *Acta Crystallogr.* **1988**, *A44*, 216–222.
(14) Wilkins, S. W.; Varghese, J. N.; Lehmann, M. S. *Acta Crystallogr.* **1983**, *A39*, 47–60.
(15) Potton, J. A.; Daniell, G. J.; Rainford, B. D. *J. Appl. Cryst.* **1988**, *21*, 663–668.
(16) Stephenson, D. S. *Prog. Nucl. Magn. Reson. Spectrosc.* **1988**, *20*, 515–626.
(17) Parker, R. L. *Rev. Earth Planet Sci.* **1977**, *5*, 272–304.
(18) Potton, J. A.; Daniell, G. J.; Melville, D. *J. Phys.* **1984**, *D17*, 1567–1581.
(19) Byran, R. K. *Eur. Biophys. J.* **1990**, *18*, 165–174.
(20) Skilling, J., Ed. *Maximum Entropy and Bayesian Methods*; Kluwer: Dordrecht, 1989.
(21) Smith, C. R., Erickson, G. J., Eds. *Maximum Entropy and Bayesian Spectral Analysis and Estimation Problems*; Kluwer: Dordrecht, 1987.
(22) Provencher, S. *CONTIN Users Manual*; Technical Report EMBLDA07; Heidelberg, 1984.
(23) Toutenburg, H., Ed. *Prior Information in Linear Models*; Wiley: Chichester, 1982.
(24) Levenberg, K. *O. Appl. Math.* **1944**, *2*, 164–168.
(25) Burch, S. F.; Gull, S. F.; Skilling, J. *Comp. Vis. Grap. Image. Proc.* **1983**, *23*, 113–128.
(26) Skilling, J.; Bruan, R. K. *Mon. Not. R. Astr. Soc.* **1984**, *211*, 111–124.
(27) Bevington, P. R., Ed. *Data Reduction and Error Analysis for The Physical Sciences*; McGraw-Hill: New York, 1969.
(28) Ehrenberg, A. S. C., Ed. *A Primer in Data Reduction*; Wiley: New York, 1982.
(29) Taylor, J. R., Ed. *An Introduction to Error Analysis*; University Science Books: Mill Valley, CA, 1982.
(30) Wang, Z. L.; Chu, B.; Wang, Q.-W.; Fetters, L. *New Trends In Physics And Physical Chemistry of Polymers*; Lee, L.-H., Ed.; Plenum: New York, 1989; pp 207–228.

Registry No. PS (homopolymer), 9003-53-6; PMMA (homopolymer), 9011-14-7.